

# Anion substitution in $\text{Ca}(\text{BH}_4)_2\text{-CaI}_2$ : Synthesis, structure and stability of three new compounds

Line H. Rude,<sup>1</sup> Yaroslav Filinchuk,<sup>1,2,3,\*</sup> Magnus H. Sørby,<sup>4</sup> Bjørn C. Hauback,<sup>4</sup>  
Flemming Besenbacher,<sup>5</sup> Torben R. Jensen<sup>1,\*</sup>

<sup>1</sup> Center for Materials Crystallography (*CMC*), Interdisciplinary Nanoscience Center (*iNANO*) and Department of Chemistry, Aarhus University, Langelandsgade 140, DK-8000 Århus C, Denmark.

<sup>2</sup> Swiss-Norwegian Beam Lines at ESRF, BP-220, 38043 Grenoble, France

<sup>3</sup> Institute of Condensed Matter and Nanosciences, Université Catholique de Louvain, place L. Pasteur 1, B-1348 Louvain-la-Neuve, Belgium

<sup>4</sup> Institute for Energy Technology, P. O. Box 40 Kjeller, NO-2027, Norway

<sup>5</sup> Interdisciplinary Nanoscience Center (*iNANO*) and Department of Physics and Astronomy, Aarhus University, DK-8000 Aarhus C, Denmark.

\* Corresponding authors: [Yaroslav.Filinchuk@uclouvain.be](mailto:Yaroslav.Filinchuk@uclouvain.be) and [trj@chem.au.dk](mailto:trj@chem.au.dk), Tel: +45 8942 3894, Fax: +45 8619 6199

## Abstract

The substitution of the complex borohydride anion  $\text{BH}_4^-$  in calcium borohydride by the larger iodide anion  $\text{I}^-$  is explored in order to tailor the hydrogen storage properties. Three new compounds are identified in the  $\text{Ca}(\text{BH}_4)_2\text{-CaI}_2$  system and are structurally characterized using the Rietveld method and synchrotron radiation powder X-ray diffraction (SR-PXD) data. Calcium borohydride readily dissolves in the trigonal calcium iodide structure during ball milling, forming a solid solution  $\text{Ca}((\text{BH}_4)_{1-x}\text{I}_x)_2$  with a  $\text{CaI}_2$ -type structure and an anisotropically contracted trigonal unit cell,  $a = 4.311(1)$  and  $c = 6.867(2)$  Å for  $x \sim 0.3$  ( $T = 28$  °C), space group  $P-3m1$ . The trigonal *tri*- $\text{Ca}((\text{BH}_4)_{0.70}\text{I}_{0.30})_2$  transforms at  $\sim 180$  °C to an orthorhombic phase of similar composition, *ort*- $\text{Ca}((\text{BH}_4)_{0.64}\text{I}_{0.36})_2$ , with a  $\text{CaCl}_2$ -type structure (a distorted  $\beta$ - $\text{Ca}(\text{BH}_4)_2$  type structure) and cell parameters  $a = 7.271(2)$ ,  $b = 7.042(1)$  and  $c = 4.4601(7)$  Å ( $T = 322$  °C), space group  $Pnmm$ . Further heating of the  $\text{CaCl}_2$ -type compound to  $\sim 330$  °C leads to a transition to a tetragonal phase with cell parameters  $a = 4.1062(2)$  and  $c = 24.822(2)$  Å ( $T = 340$  °C,  $x \sim 0.62$ ), space group  $I4mm$ . This iodide-rich compound *tet*- $\text{Ca}((\text{BH}_4)_{0.38}\text{I}_{0.62})_2$ , has a new structure type. The tetragonal phase finally decomposes to  $\text{CaHI}$  and  $\text{CaB}_6$  at  $T > 345$  °C. All three novel compounds found in the  $\text{Ca}(\text{BH}_4)_2\text{-CaI}_2$  system are stable at *RT*. The anion substitution ultimately changes the decomposition reaction pathway in which hydrogen is released from a tetragonal  $\text{Ca}((\text{BH}_4)_{1-x}\text{I}_x)_2$  via  $\text{CaHI}$ , but unfortunately the temperature of hydrogen release is still fairly high and similar to that for  $\text{Ca}(\text{BH}_4)_2$ .

## 1. Introduction

Renewable energy sources are an environmentally friendly, inexhaustible alternative to fossil fuels, but their utilization are hampered since the energy production generally fluctuates in time and is non-uniformly distributed geographically. The solution should be a safe, cheap and efficient energy carrier, and hydrogen is a world-wide target receiving increasing political and scientific interest.<sup>1</sup> The characteristics of the ideal hydrogen storage material for mobile applications are high gravimetric and volumetric hydrogen content, the ability to store hydrogen reversibly with fast hydrogen release and uptake kinetics at moderate temperatures, low heat exchange and prepared from abundant, inexpensive and robust materials.<sup>2-4</sup> At present, no single material fulfills all these requirements.<sup>5-7</sup>

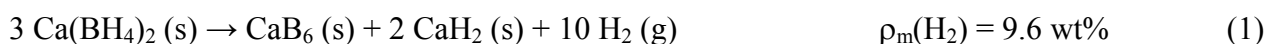
Light metal borohydrides currently receive considerable interest due to their high gravimetric hydrogen contents, *e.g.* 18.5 wt% for LiBH<sub>4</sub>.<sup>8</sup> Unfortunately, the utilization of borohydrides for practical applications is often hampered by limited reversibility, unfavorable kinetics and thermodynamics.<sup>6,8</sup> Several novel materials have recently been synthesized, *e.g.* LiSc(BH<sub>4</sub>)<sub>4</sub>, NaSc(BH<sub>4</sub>)<sub>4</sub>, and KSc(BH<sub>4</sub>)<sub>4</sub> with the complex anion [Sc(BH<sub>4</sub>)<sub>4</sub>]<sup>-</sup>,<sup>9-12</sup> LiZn<sub>2</sub>(BH<sub>4</sub>)<sub>5</sub> and NaZn<sub>2</sub>(BH<sub>4</sub>)<sub>5</sub> with interpenetrated networks, NaZn(BH<sub>4</sub>)<sub>3</sub>,<sup>13</sup> containing polymeric anions, and KZn(BH<sub>4</sub>)Cl<sub>2</sub>,<sup>14</sup> with heteroleptic composite anions. These compounds release hydrogen at low temperatures but, in some cases irreversibly parallel with release of borane gases.<sup>15</sup> This was also observed although in small amounts for the more stable ionic borohydrides, *e.g.* LiBH<sub>4</sub>.<sup>16</sup> Bi-metallic alkali transition metal borohydrides based on the early *d*-block metals, *e.g.* Sc and Y, clearly have the ability to form stable boron compounds in the solid state, *i.e.* avoiding the release of borane gases.<sup>9-12,17-19</sup> Metal borohydrides may also crystallize with partly open structures as observed for Mn(BH<sub>4</sub>)<sub>2</sub> and  $\alpha$ -Mg(BH<sub>4</sub>)<sub>2</sub>, which reveal a large structural flexibility for the borohydride materials.<sup>8,20,21</sup> The properties of known borohydrides may be improved by chemical

reactions as realized in reactive hydride composites (RHC), which have the weighted average hydrogen storage capacity as compared to the individual components but may have significantly improved thermodynamic properties as observed for the  $2\text{LiBH}_4\text{-MgH}_2$  system.<sup>22-26</sup> Another approach is anion substitution, which may modify the physical properties of the hydrogen storage material. Theoretical calculations suggest that the substitution of the hydride ion with the more electronegative fluorine ion, *i.e.*  $\text{H}^- \rightarrow \text{F}^-$ , will significantly alter the hydrogen release and uptake properties for the  $\text{BH}_4^-$  ion, *e.g.* in  $\text{LiBH}_4$ .<sup>27</sup> Fluorine substitution has been performed experimentally in aluminum based alanates, *e.g.*  $\text{NaAlH}_4$ ,<sup>28-32</sup> resulting in a destabilization of the material. The heavier halides readily substitute in borohydrides and form solid-solution or stoichiometric compounds, *e.g.*  $\text{Cl}^-$ ,  $\text{Br}^-$  or  $\text{I}^-$  can substitute for  $\text{BH}_4^-$  in  $\text{LiBH}_4$  or  $\text{Ca}(\text{BH}_4)_2$ .<sup>33-36</sup> By the choice of anion species and the extent of the substitution, it may be possible to modify the conditions for hydrogen uptake and release. Furthermore, anion-substituted borohydrides have significantly improved lithium ion conduction properties.<sup>33</sup>

Calcium borohydride,  $\text{Ca}(\text{BH}_4)_2$ , has a high theoretical hydrogen content calculated both gravimetrically,  $\rho_m = 11.6 \text{ wt\% H}_2$ , and volumetrically,  $\rho_v = 108 \text{ g H}_2/\text{L}$ , and receives increasing interest for utilization as a possible hydrogen storage material.<sup>37-39</sup> Calcium borohydride exhibits interesting structural chemistry with at least four known polymorphs denoted  $\alpha$ -,  $\beta$ -,  $\gamma$ - and  $\alpha'$ - $\text{Ca}(\text{BH}_4)_2$ ,<sup>8,38,40-45</sup> where up to three polymorphs  $\alpha$ -,  $\beta$ - and  $\gamma$ - $\text{Ca}(\text{BH}_4)_2$  may coexist under ambient conditions. The stable room temperature (*RT*) polymorph is orthorhombic  $\alpha$ - $\text{Ca}(\text{BH}_4)_2$  with space group symmetry  $F2dd$  (no. 43).<sup>40</sup> A transformation to the high-temperature  $\beta$ - $\text{Ca}(\text{BH}_4)_2$  phase occurs at  $T > 176 \text{ }^\circ\text{C}$ . Different space group symmetries have been suggested for the  $\beta$ -phase,  $P4_2/m$  (no. 84),<sup>41,46</sup>  $P4_2nm$  (no. 102) and  $P-4$  (no. 81),<sup>40</sup> but all structural models are similar.  $\beta$ - $\text{Ca}(\text{BH}_4)_2$  is meta-stable at *RT* and slowly transforms to the  $\alpha$ -phase upon cooling.<sup>40,47</sup> The orthorhombic  $\gamma$ -

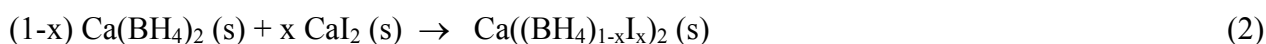
Ca(BH<sub>4</sub>)<sub>2</sub> with the space group symmetry *Pbca* (no. 61)<sup>44,48</sup> transforms to β-Ca(BH<sub>4</sub>)<sub>2</sub> at 290 °C. A second order phase transition from α- to the tetragonal α'-Ca(BH<sub>4</sub>)<sub>2</sub>, space group *I-42d* (no. 122), can be observed at 222 °C.<sup>40</sup>

Calcium borohydride decomposes in the temperature range from 360 to 500 °C, releasing 9.6 wt% hydrogen via reaction (1).<sup>37,38,42,48,49</sup>



Partial rehydrogenation has been demonstrated at  $p(\text{H}_2) = 90$  bar and at 350 to 420 °C using the proper additives.<sup>39,50</sup>

The high decomposition temperature makes calcium borohydride unsuitable for practical hydrogen storage applications,<sup>38</sup> and it is therefore tempting to modify the thermodynamics and kinetics of hydrogen release and uptake using partial anion substitution. This has prompted us to study the substitution of the complex anion BH<sub>4</sub><sup>-</sup> by the larger iodide anion, I<sup>-</sup>, as described in reaction scheme (2),



Here we present synthesis, crystal structures, and thermal transformation of three new iodide-substituted calcium borohydrides investigated by *in situ* synchrotron radiation powder X-ray diffraction along with an investigation of their hydrogen storage properties.

## 2. Experimental

### 2.1 Sample preparation

Calcium borohydride was prepared from commercially available  $\text{Ca}(\text{BH}_4)_2 \cdot 2\text{THF}$  (Aldrich) by desolvating in vacuum ( $p \approx 10^{-1}$  mbar) for 24 hours at 170 °C, denoted TT (thermal treatment) in Table 1. The obtained product, denoted **R1**, was a mixture of  $\alpha$ - and  $\beta$ - $\text{Ca}(\text{BH}_4)_2$ . A sample of  $\alpha$ - $\text{Ca}(\text{BH}_4)_2$ , denoted **R2**, was produced by ball milling (BM) a fraction of **R1** for 2 hours at 250 rpm (2 min, 2 min break, 60 repetitions) and with a sample to ball ratio of approximately 1 : 30. The vial was sealed with a lid and a teflon O-ring under purified argon atmosphere.

Sample R1,  $\alpha$ - and  $\beta$ - $\text{Ca}(\text{BH}_4)_2$  was mixed with  $\text{CaI}_2$  (Aldrich, 99.999%) in molar ratios of 1 : 0.22, producing a sample denoted **S1**, 1 : 0.42 (**S2**), or 1 : 0.86 (**S4**) and ball milled using the procedure described above. A similar sample in the molar ratio 1 : 0.42 (**S3**) was hand-mixed (HM) for 10 min in an agate mortar. The investigated samples are listed in Table 1. All handling and manipulation of the chemicals and sample preparations were performed in an argon-filled glove box with circulation purifier,  $p(\text{O}_2, \text{H}_2\text{O}) < 0.5$  ppm.

**Table 1.** List of investigated samples. The composition of the samples is given as the molar ratios and the molar fractions,  $n(\text{CaI}_2)/n(\text{total})$ . The preparation methods are either ball milling (BM), hand-mixing in a mortar (HM) or thermal treatment (TT) in argon atmosphere.

Notation	Materials	Molar ratio	$n(\text{CaI}_2)/n(\text{total})$	Preparation
<b>R1</b>	$\alpha$ - and $\beta$ - $\text{Ca}(\text{BH}_4)_2$	-	0	TT <sup>a</sup>
<b>R2</b>	$\alpha$ - $\text{Ca}(\text{BH}_4)_2$	-	0	TT <sup>a</sup> and BM
<b>S1</b>	$\text{Ca}(\text{BH}_4)_2 + \text{CaI}_2$	1 : 0.22	0.18	BM
<b>S2</b>	$\text{Ca}(\text{BH}_4)_2 + \text{CaI}_2$	1 : 0.42	0.29	BM
<b>S3</b>	$\text{Ca}(\text{BH}_4)_2 + \text{CaI}_2$	1 : 0.42	0.29	HM
<b>S4</b>	$\text{Ca}(\text{BH}_4)_2 + \text{CaI}_2$	1 : 0.86	0.46	BM

<sup>a</sup> 170 °C / 24 h cooled naturally in air to RT.

## 2.2 *In situ* synchrotron radiation powder X-ray diffraction

*In situ* synchrotron radiation powder X-ray diffraction (SR-PXD) data for the samples **S1**, **S2**, **S3** and **S4** were measured at the beamline BM01A at the Swiss-Norwegian Beam Lines (SNBL), European Synchrotron Radiation Facility (ESRF), Grenoble, France, using a MAR345 image plate detector. The samples were mounted in glass capillaries sealed with a composite adhesive in an argon atmosphere (1 bar) to prevent contact with air.<sup>51</sup> The data were collected at a sample-to-detector distance of 275 mm (**S1**, **S2** and **S3**) and 200 mm (**S4**), and the capillaries were rotated 20° during the data collection. The X-ray exposure time for each powder pattern was 20 s using selected wavelengths of  $\lambda = 0.703511 \text{ \AA}$  (**S1** and **S3**),  $\lambda = 0.6548 \text{ \AA}$  (**S2**) and  $\lambda = 0.721082 \text{ \AA}$  (**S4**). The wavelength and the detector geometry were calibrated using an external standard, LaB<sub>6</sub>. Decomposition reactions were investigated in the temperature range from *RT* to 360 °C for samples **S1** and **S3**, and from *RT* to 400 °C for samples **S2** and **S4** using heating rates of 3, 4, 2 and 2 °C/min, respectively.

The data were integrated using the Fit2D program,<sup>52</sup> uncertainties for the integrated intensities were calculated using each 2 $\theta$ -point taking the geometry of the detector into consideration.<sup>53</sup> The relative amounts of the different phases in the investigated samples were estimated by integrating the intensity of selected Bragg reflections applying a Gaussian fit and subtracting the background intensity by use of a linear interpolation. The integrated intensities are normalized and shown as a function of temperature (The intensity,  $\alpha(t) = I_i(t) / I_{i,\max}$ , for the compound *i* at the time *t*). The unit cell parameters were determined with the DICVOL2004 software,<sup>54</sup> and structural models were obtained using direct space algorithms implemented in the program FOX.<sup>55</sup> The structural models were refined with the Rietveld methods in the Fullprof suite.<sup>56</sup> The sequential refinement of the *in situ* SR-PXD data was performed to follow the change in composition and unit cell volumes.

Previously published structural parameters were used as an initial input for the Rietveld refinements when available.<sup>40,57-59</sup>

### 2.3 Thermal analysis

Differential scanning calorimetry (DSC) and thermogravimetric analysis (TGA) were performed simultaneously with a Netzsch STA449C Jupiter instrument at heating and cooling rates of 10.0 °C/min in a flow of He (50 mL/min) for the samples **R1**, **S1** and **S2**. Prior to the experiment the samples were heated to 300 °C and cooled to *RT* three times in order to investigate the dynamic properties of the substitution process. The fourth heating was continued to 550 °C to determine the hydrogen release. The samples were mounted in Al<sub>2</sub>O<sub>3</sub> crucibles with tiny holes in the lid to prevent increase in pressure during desorption of gases.

Sieverts measurements were recorded with a PCTpro 2000 instrument from Hy-Energy.<sup>60</sup> The samples were loaded in an autoclave and sealed in argon atmosphere. Temperature-pressure desorption (TPD) experiments were performed in the temperature range from *RT* to 550 °C with a heating rate of 0.5 °C/min in vacuum. Hydrogen absorption data were measured in the temperature range *RT* to 350 °C (20 °C/min) followed by 10 hours at the fixed temperature of 350 °C. A hydrogen pressure of ca. 100 bar was initially applied.

## 3. Results and discussion

To study the substitution of CaI<sub>2</sub> into Ca(BH<sub>4</sub>)<sub>2</sub>, four different samples (**S1-4**, see Table 1) were prepared and characterized by *in situ* SR-PXD at variable temperatures to probe the mechanism for

the substitution and the structural chemistry of the different phases. Three new compounds were found in the  $\text{Ca}(\text{BH}_4)_2\text{-CaI}_2$  system and structurally characterized as summarized in Table 2.

**Table 2** The crystal system, unit cell parameters and space group for the three new compounds found in this study compared to selected known compounds. The X-ray data collection temperature is given for comparison.

Structure	Crystal system	Space group	$a / \text{\AA}$	$b / \text{\AA}$	$c / \text{\AA}$	$V / \text{\AA}^3$	$T / ^\circ\text{C}$
$\alpha\text{-Ca}(\text{BH}_4)_2$ <sup>40</sup>	Orthorhombic	$F2dd$	8.7759(3)	13.0234(4)	7.4132(2)	847.27	-183
$\beta\text{-Ca}(\text{BH}_4)_2$ <sup>40</sup>	Tetragonal	$P4_2nm$ or $P-4$	6.91894(11)		4.34711(12)	208.10	222
$\beta\text{-Ca}(\text{BH}_4)_2$ <sup>41</sup>	Tetragonal	$P4_2/m$	6.9468(1)		4.3661(1)	210.70	207
$\text{CaI}_2$ <sup>57</sup>	Trigonal	$P-3m1$	4.49(2)		6.975(30)	121.78	$RT$
$\text{CaCl}_2$ <sup>59</sup>	Orthorhombic	$Pnmm$	6.24	6.43	4.2	168.52	$RT$
$\text{CaHI}$ <sup>58</sup>	Tetragonal	$P4/nmm$	4.071		8.941	148.18	$RT$
$tri\text{-Ca}((\text{BH}_4)_{0.70}\text{I}_{0.30})_2$ <sup>a</sup>	Trigonal	$P-3m1$	4.3107(11)		6.8669(19)	110.51	28
$ort\text{-Ca}((\text{BH}_4)_{0.64}\text{I}_{0.36})_2$ <sup>a</sup>	Orthorhombic	$Pnmm$	7.2713(15)	7.04182(12)	4.4600(6)	228.37	322
$tet\text{-Ca}((\text{BH}_4)_{0.38}\text{I}_{0.62})_2$ <sup>a</sup>	Tetragonal	$I4mm$	4.1067(2)		24.821(2)	418.51	340

<sup>a</sup>This work

### 3.1 Structural investigation of three new compounds observed in the $\text{Ca}(\text{BH}_4)_2\text{-CaI}_2$ system

A set of relatively broad Bragg peaks are observed at  $RT$  for all ball-milled  $\text{Ca}(\text{BH}_4)_2\text{-CaI}_2$  samples (**S1**, **S2**, **S4**). These reflections were indexed with a trigonal unit cell, similar to the one for the  $\text{CaI}_2$  structure. Global structural optimization using the program FOX and space group  $P-3m1$  and followed by Rietveld refinement showed that the  $\text{Ca}(\text{BH}_4)_2\text{-CaI}_2$  (0.71:0.29, **S2**) mixture became a single phase with a  $\text{CaI}_2$ -type structure and a refined iodide concentration of 0.30(2), *i.e.*  $tri\text{-Ca}((\text{BH}_4)_{0.70}\text{I}_{0.30})_2$ , in agreement with the nominal composition. The Rietveld refinement converged at  $R_B = 4.18\%$ ,  $R_F = 3.18\%$ ,  $R_p = 10.5\%$  and  $R_{wp} = 11.6\%$  (conventional indexes, these are more correct values as the fit to the background is not included) and  $R_p = 2.46\%$  and  $R_{wp} = 3.21\%$  (not corrected for background). The observed and calculated PXD profiles are shown in Figure 1, and

the structure of the trigonal solid solution is illustrated in Figure 2. Atomic coordinates and selected bond lengths are given in the supplementary information (see Tables s1 and s2).

Calcium cations in the trigonal, *tri*-Ca((BH<sub>4</sub>)<sub>0.70</sub>I<sub>0.30</sub>)<sub>2</sub>, structure are octahedrally coordinated by six anions (I<sup>-</sup> or BH<sub>4</sub><sup>-</sup>), CN(Ca) = 6. Each anion is coordinated to three Ca atoms (CN = 3) situated in the base of a trigonal pyramid. On the other side, the anion is pointing to the middle of the triangle formed by iodide/BH<sub>4</sub><sup>-</sup> units of the neighboring layer (see Figure 2) and the anion-anion distances are 4.197(6) Å. The cation–anion distances in the BH<sub>4</sub>-substituted compound are slightly shorter than in CaI<sub>2</sub>, *i.e.* 3.039(3) and 3.124(6) Å, respectively.<sup>57</sup> The unit cell volume per formula unit, *V*/*Z*, clearly decreases as a consequence of dissolution of Ca(BH<sub>4</sub>)<sub>2</sub> in CaI<sub>2</sub>, *i.e.* from 121.8 to 110.5 Å<sup>3</sup> for CaI<sub>2</sub> and Ca((BH<sub>4</sub>)<sub>0.70</sub>I<sub>0.30</sub>)<sub>2</sub>, respectively, which correlates with the size of the respective anions.<sup>61</sup>

Further heating of the trigonal solid solution, *tri*-Ca((BH<sub>4</sub>)<sub>0.70</sub>I<sub>0.30</sub>)<sub>2</sub> obtained from sample **S2** leads to the formation of a new compound observed at ~180 °C. The new set of Bragg reflections was indexed by an orthorhombic unit cell, and a structural model was created in the space group *Pnnm* using FOX.<sup>55</sup> The resulting structural model is a CaCl<sub>2</sub>-type structure, with the site of the anion statistically occupied by iodide ions and borohydride complexes. The refined composition *ort*-Ca((BH<sub>4</sub>)<sub>0.64</sub>I<sub>0.36</sub>)<sub>2</sub> of the single-phase sample (*T* = 322 °C, **S2**) is similar to the composition of the trigonal phase. Rietveld refinement of the structural model converged at *R*<sub>B</sub> = 7.69% and *R*<sub>wp</sub> = 11.3% (conventional indexes) and *R*<sub>wp</sub> = 2.91% (not corrected for background). The observed and calculated profiles are shown in Figure 3, and the structure of the orthorhombic phase is illustrated in Figure 4. Atomic coordinates and selected bond lengths are given in the supplementary

information (see Tables s3 and s4). The orthorhombic phase is stable upon cooling to room temperature.

Calcium cations in the orthorhombic solid solution have octahedral coordination (CN = 6) to six  $\text{BH}_4^-$  or  $\text{I}^-$  ions. However, the anion sites have a different environment, namely trigonal-planar (CN = 3) as compared to the trigonal pyramidal coordination in the trigonal phase. The resulting structure is not layered but polymeric in all three dimensions (see Figure 4). The Ca-anion distance is 2.967(3) and 3.026(2) Å at *RT*, which is significantly longer than the Ca-Cl distances in  $\text{CaCl}_2$ , 2.70(5) to 2.76(3) Å at *RT*, due to the larger radius of  $\text{I}^-$  and  $\text{BH}_4^-$  ions as compared to  $\text{Cl}^-$  ions. The shortest anion-anion distances are 4.166(5) and 3.59(7) Å in the orthorhombic solid solution and  $\text{CaCl}_2$ , respectively, see Table 3.

The symmetry of the orthorhombic phase shows an interesting aspect with respect to the iodide-free  $\beta\text{-Ca}(\text{BH}_4)_2$ . Similar to  $\text{CaCl}_2$ , which undergoes a second order phase transition from a *Pnmm* to a *P4<sub>2</sub>/mnm* phase on heating,<sup>62</sup> the former is a distortion of the latter. The actual symmetry of a number of *Pnmm* structures, known as  $\text{FeS}_2$ -type structures, can be lower, namely *Pnn2*.<sup>63</sup> Therefore, a group-subgroup relation between the *ort*- $\text{Ca}((\text{BH}_4)_{1-x}\text{I}_x)_2$  (*Pnmm*) and the tetragonal  $\beta\text{-Ca}(\text{BH}_4)_2$  phase holds only for one of the three space group symmetries (*P4<sub>2</sub>/m*,<sup>41</sup> *P4<sub>2</sub>nm* or *P-4*<sup>40</sup>) suggested for the  $\beta\text{-Ca}(\text{BH}_4)_2$  structures, *i.e.* *Pnn2*  $\leftrightarrow$  *P4<sub>2</sub>nm*. The *P4<sub>2</sub>nm* symmetry also corresponds with the observed systematic absences in the diffraction data.<sup>40</sup> We attempted to refine the orthorhombic  $\text{Ca}((\text{BH}_4)_{1-x}\text{I}_x)_2$  structure in the space group *Pnn2*, but with no obvious improvement of the fit. This argument alone cannot rule out the lower symmetry, since the differentiation between the two space groups from diffraction data was shown to be a challenge,<sup>64</sup> and the apparent deviation from the centrosymmetric *Pnmm* model appears to be small for other  $\text{AB}_2$  systems.<sup>63</sup> The  $\text{BH}_4^-$  groups in  $\beta\text{-Ca}(\text{BH}_4)_2$  may be intrinsically disordered, similar to the high-temperature hexagonal polymorph of  $\text{LiBH}_4$ ,<sup>65</sup> which may contribute to the difficulties in

theoretical description of the structure using a harmonic approximation<sup>66</sup> or experimentally using powder diffraction data.<sup>40,41</sup>

Further heating of the CaCl<sub>2</sub>-type solid solution, *ort*-Ca((BH<sub>4</sub>)<sub>0.64</sub>I<sub>0.36</sub>)<sub>2</sub> (322 °C, **S2**), provides another new powder diffraction profile observed at 335 °C. The new solid solution is observed in a temperature interval from 335 to ~400 °C, but already starts to decompose at ~345 °C. The highest quality diffraction pattern is collected at 340 °C for a sample (**S2**) containing a mixture of the CaCl<sub>2</sub>-type solid solution and the new phase, see Figure 5. This data allows indexing the new set of diffraction peaks with a tetragonal cell,  $a = b = 4.1067(2)$  and  $c = 24.821(2)$  Å, and was used for structure determination. Systematic absences suggest a body-centered cell, and the global optimization in FOX yielded a reasonable structure in the space group *I4mm*. The presented structural model is only tentative and still needs to be confirmed or revised by other methods. The structure contains two Ca atom sites and four sites occupied by I<sup>-</sup> and BH<sub>4</sub><sup>-</sup> anions. Two of them (I1 and I2) appear to be fully occupied by I<sup>-</sup>, and the other two (I3 and I4) by a statistical mixture of borohydride and iodide anions. The Rietveld refinement converged at  $R_B = 8.74\%$ ,  $R_F = 7.49\%$ ,  $R_p = 15.8\%$ ,  $R_{wp} = 16.1\%$  (conventional indexes) and  $R_p = 2.79\%$  and  $R_{wp} = 3.73\%$  (not corrected for background). The refined composition for the new tetragonal *I4mm* structure is *tet*-Ca((BH<sub>4</sub>)<sub>0.38</sub>I<sub>0.62</sub>)<sub>2</sub> (340 °C, **S2**), and the sample contained only 20 wt% of this phase, and 80 wt% of the *ort*-Ca((BH<sub>4</sub>)<sub>0.61</sub>I<sub>0.39</sub>)<sub>2</sub> (340 °C, **S2**). The observed and calculated profiles are shown in Figure 5, and the structure of the tetragonal phase is illustrated in Figure 6. Atomic coordinates and selected bond lengths are given in the supplementary information (see Tables s5 and s6).

The tetragonal *I4mm* phase has a long *c*-axis as compared to the cell parameters in the *a,b* basal plane and to other similar compounds (see Table 2). The structure is relatively rich in iodide and is built of layers similar to the CaI<sub>2</sub> structure. However, the coordination numbers for Ca atoms differ significantly. Ca1 site has a slightly distorted cubic environment (CN = 8) with Ca-anion distances

in the range 3.35(2) to 3.70(4) Å, while Ca2 site has a tetragonal-pyramidal coordination (CN = 5) with significantly shorter distances of 2.79(3)-3.026(13) Å. As illustrated in Figure 6, the layers of cubic and pyramidal coordination alter along the *c*-axis, forming the I2...I3 contact of 3.43(2) Å. This distance is somewhat shorter compared to the other distances between the anions, which are closer to the expected values of ~4.0 Å. The shortest Ca-anion and anion-anion distances for the new compounds observed in this study and for selected known phases are listed in Table 3.

**Table 3.** Essential interatomic distances determined from diffraction data measured at different temperatures for the three new compounds observed in this study and for selected known compounds.

Compound	Anion	Ca...Anion /Å	Shortest Anion...Anion /Å	T/°C
$\alpha$ -Ca(BH <sub>4</sub> ) <sub>2</sub> <sup>40</sup>	BH <sub>4</sub> <sup>-</sup>	2.816(8)-2.967(8)	3.648(11)	-183
$\beta$ -Ca(BH <sub>4</sub> ) <sub>2</sub> <sup>40</sup>	BH <sub>4</sub> <sup>-</sup>	2.923(8)-2.939(8)	3.80(2)	32
CaI <sub>2</sub> <sup>57</sup>	I <sup>-</sup>	3.124(6)	4.345(12)	RT
CaCl <sub>2</sub> <sup>59</sup>	Cl <sup>-</sup>	2.70(5)-2.76(3)	3.59(7)	RT
<i>tri</i> -Ca((BH <sub>4</sub> ) <sub>0.70</sub> I <sub>0.30</sub> ) <sub>2</sub> <sup>a</sup>	I <sup>-</sup> /BH <sub>4</sub> <sup>-</sup>	3.039(3)	4.197(6)	44
<i>ort</i> -Ca((BH <sub>4</sub> ) <sub>0.64</sub> I <sub>0.36</sub> ) <sub>2</sub> <sup>a</sup>	I <sup>-</sup> /BH <sub>4</sub> <sup>-</sup>	3.007(3)-3.057(2)	4.181(4)	322
<i>tet</i> -Ca((BH <sub>4</sub> ) <sub>0.38</sub> I <sub>0.62</sub> ) <sub>2</sub> <sup>a</sup>	I <sup>-</sup> /BH <sub>4</sub> <sup>-</sup>	2.79(3)-3.70(4)	3.43(2)	340

<sup>a</sup> This work

### 3.2 *In situ* SR-PXD characterization of the system Ca(BH<sub>4</sub>)<sub>2</sub>-CaI<sub>2</sub>

A series of *in situ* SR-PXD patterns of a ball-milled sample of Ca(BH<sub>4</sub>)<sub>2</sub>-CaI<sub>2</sub> (0.82 : 0.18, **S1**) is shown in Figure 7 in the temperature range 44 °C to 400 °C (2 °C/min). The first pattern includes Bragg reflections from the reactants  $\alpha$ - and  $\beta$ -Ca(BH<sub>4</sub>)<sub>2</sub> and CaI<sub>2</sub> and a number of broad reflections from the trigonal, *tri*-Ca((BH<sub>4</sub>)<sub>0.61</sub>I<sub>0.39</sub>)<sub>2</sub> (44 °C, **S1**), solid solution. This indicates that calcium borohydride dissolves in the structure of calcium iodide during the mechano-chemical treatment,

*i.e.* ball milling. Rietveld refinement of the  $\beta$ -Ca(BH<sub>4</sub>)<sub>2</sub> structure revealed no iodide substitution at  $T = 44$  °C within the experimental uncertainty.

Several reactions occur, in some cases simultaneously or as coupled chemical reactions, during heating of the sample as discussed in the following. This is visualized by integrating selected well-resolved reflections from observed phases. The data is shown in Figure 8 as normalized integrated intensities for the temperature range from 250 to 400 °C to obtain an overview of the sample composition as a function of temperature.

The second order phase transition  $\alpha$ - to  $\alpha'$ -Ca(BH<sub>4</sub>)<sub>2</sub> is observed in Figure 7 at 222 °C, following an increase in the  $a$ -axis unit cell parameter simultaneously with a decrease in the  $b$ -axis parameter over a broad temperature range.<sup>40</sup> Further heating results in the formation of  $\beta$ -Ca(BH<sub>4</sub>)<sub>2</sub> from  $\alpha'$ -Ca(BH<sub>4</sub>)<sub>2</sub> and the polymorphic transformations are summarized in the reaction scheme (3).



The  $\alpha'$ -phase is completely transformed to  $\beta$ -Ca(BH<sub>4</sub>)<sub>2</sub> at  $\sim 270$  °C. The gradual structural transformation from *tri*-Ca((BH<sub>4</sub>)<sub>1-x</sub>I<sub>x</sub>)<sub>2</sub> to the orthorhombic, *ort*-Ca((BH<sub>4</sub>)<sub>1-x</sub>I<sub>x</sub>)<sub>2</sub>, solid solution is observed in the temperature range 150 to 313 °C. The refined iodide content of *ort*-Ca((BH<sub>4</sub>)<sub>0.77</sub>I<sub>0.23</sub>)<sub>2</sub> ( $T = 313$  °C, **S1**) is lower than the iodide content in the trigonal phase, indicating that the orthorhombic phase is formed by dissolving  $\beta$ -Ca(BH<sub>4</sub>)<sub>2</sub> in the trigonal phase.

However, most diffraction peaks from the tetragonal  $\beta$ -Ca(BH<sub>4</sub>)<sub>2</sub> and the *ort*-Ca((BH<sub>4</sub>)<sub>1-x</sub>I<sub>x</sub>)<sub>2</sub> coincide, and the two compounds can only be distinguished by differences in the relative Bragg peak intensities and splitting of the reflections. The splitting is due to the expansion of the *ort*-Ca((BH<sub>4</sub>)<sub>0.77</sub>I<sub>0.23</sub>)<sub>2</sub> (313 °C, **S1**) unit cell by the iodide substitution and a small difference in  $a$  and  $b$  unit cell parameters.

The PXD patterns at 300 °C contain only diffraction peaks from the *ort*-Ca((BH<sub>4</sub>)<sub>0.77</sub>I<sub>0.23</sub>)<sub>2</sub> (313 °C, **S1**) and CaI<sub>2</sub>. The intensity of some CaI<sub>2</sub> reflections decreases in the temperature range 250 to ~360 °C simultaneously with an increase in the *ort*-Ca((BH<sub>4</sub>)<sub>0.77</sub>I<sub>0.23</sub>)<sub>2</sub> (313 °C, **S1**), see Figure 8, however no significant change in the composition of *ort*-Ca((BH<sub>4</sub>)<sub>0.77</sub>I<sub>0.23</sub>)<sub>2</sub> (313 °C, **S1**) was observed by Rietveld refinement of the X-ray data. On the other hand, some Bragg reflections, *e.g.* peaks at 11.43, 17.82, 21.24° 2 $\theta$ , of the CaI<sub>2</sub> phase increase in intensity, which may be due to the formation of an unknown high temperature polymorph of CaI<sub>2</sub>. This unidentified phase is clearly observed in the hand-mixed sample in the same temperature range. The intensity of the orthorhombic solid solution increases until a rapid transformation at ~340 °C to the tetragonal compound, *tet*-Ca((BH<sub>4</sub>)<sub>0.35</sub>I<sub>0.65</sub>)<sub>2</sub> (361 °C, **S1**), see Figure 8, with an associated mass loss (as discussed in the following section). The tetragonal phase only exists in a narrow temperature range as the slow decomposition to CaHI and amorphous CaB<sub>6</sub> initiates at 350 °C. The formation of amorphous CaB<sub>6</sub> was observed by solid state MAS NMR and will be the focus of a future publication. Despite the decomposition of *tet*-Ca((BH<sub>4</sub>)<sub>1-x</sub>I<sub>x</sub>)<sub>2</sub>, the reflections from this phase are observed up to a temperature of 400 °C in the last SR-PXD pattern. The amount of *tet*-Ca((BH<sub>4</sub>)<sub>1-x</sub>I<sub>x</sub>)<sub>2</sub> is a balance between two chemical reactions, *i.e.* the transformation from *ort*-Ca((BH<sub>4</sub>)<sub>1-x</sub>I<sub>x</sub>)<sub>2</sub> and the decomposition to CaHI and CaB<sub>6</sub>. The largest fraction of *tet*-Ca((BH<sub>4</sub>)<sub>1-x</sub>I<sub>x</sub>)<sub>2</sub> is therefore observed at 365 °C, see Figure 8.

The *in situ* SR-PXD data for Ca(BH<sub>4</sub>)<sub>2</sub>-CaI<sub>2</sub> (0.71 : 0.29, **S2**) heated from *RT* to 360 °C are shown in Figure 9. The first PXD patterns are dominated by the relatively broad reflections from *tri*-Ca((BH<sub>4</sub>)<sub>0.70</sub>I<sub>0.30</sub>)<sub>2</sub> (*RT*, **S2**) and weak reflections from  $\alpha$ -Ca(BH<sub>4</sub>)<sub>2</sub>. A slow formation of *ort*-Ca((BH<sub>4</sub>)<sub>1-x</sub>I<sub>x</sub>)<sub>2</sub> was observed in the temperature range 160 to 322 °C by decreasing the intensity from the  $\alpha$ -Ca(BH<sub>4</sub>)<sub>2</sub> phase and by a gradual splitting of the reflection at 2 $\theta$  = 17.5°. The orthorhombic solid solution transforms to the *tet*-Ca((BH<sub>4</sub>)<sub>1-x</sub>I<sub>x</sub>)<sub>2</sub> at 335 °C, which starts to

decompose to CaHI and CaB<sub>6</sub> as observed for the sample **S1**. This is clearly observed in Figure 10, showing the integrated and normalized intensities of the observed phases for the temperature range 250 to 360 °C.

In order to investigate the influence of the preparation method on the reaction pathway, a sample of Ca(BH<sub>4</sub>)<sub>2</sub>-CaI<sub>2</sub> (0.71 : 0.29, **S3**) was prepared by hand mixing in an agate mortar, and the *in situ* SR-PXD investigation is shown in the supplementary information as Figure s1. No reaction between the pure compounds was observed at temperatures below  $T < 360$  °C, indicating that the substitution process is mediated by either the shear strain or pressure during ball milling<sup>67</sup> or by heating to temperatures above 360 °C. The transformation from  $\alpha$ - to  $\alpha'$ - and further to  $\beta$ -Ca(BH<sub>4</sub>)<sub>2</sub> was observed in the temperature range 160 to 290 °C. However, during cooling the formation of the tetragonal solid solution was observed with iodide content similar to what was observed for the samples **S1** and **S2**. Furthermore, at least one unidentified product was observed to form, with peak positions very similar to CaI<sub>2</sub> indicating that the product is a high-temperature or disordered form of CaI<sub>2</sub>. The integrated and normalized intensities for the temperature range from 100 to 360 °C are shown in the supplementary information, see Figure s2. As opposed to the other samples, the transformation from  $\alpha$ - to  $\alpha'$ -Ca(BH<sub>4</sub>)<sub>2</sub> and further to  $\beta$ -Ca(BH<sub>4</sub>)<sub>2</sub> is shown as a two-step transformation from  $\alpha$ - to  $\beta$ -Ca(BH<sub>4</sub>)<sub>2</sub> in Figure S2. A decrease in the diffracted intensity from CaI<sub>2</sub> is observed at 360 °C due to the formation of *tet*-Ca((BH<sub>4</sub>)<sub>1-x</sub>I<sub>x</sub>)<sub>2</sub>.

To explore the maximum degree of substitution, an iodide rich sample was prepared (**S4**). The *in situ* SR-PXD data measured for the sample Ca(BH<sub>4</sub>)<sub>2</sub>-CaI<sub>2</sub> (0.54 : 0.46, **S4**) heated from *RT* to 400 °C is shown in the supplementary information as Figure s3. At *RT* the sample consists of broad Bragg reflections from a *tri*-Ca((BH<sub>4</sub>)<sub>1-x</sub>I<sub>x</sub>)<sub>2</sub> phase, excess of CaI<sub>2</sub> and trace amounts of  $\alpha$ - and  $\beta$ -Ca(BH<sub>4</sub>)<sub>2</sub>. The composition of the trigonal phases cannot be found at *RT* by Rietveld refinement of

the data, however it can be estimated from the unit cell volume and appears to be similar to what was observed for the samples **S1** and **S2**, *tri*-Ca((BH<sub>4</sub>)<sub>0.7</sub>I<sub>0.3</sub>)<sub>2</sub>. The trigonal phase is observed in the temperature range from *RT* – 400 °C. However, some transformation to the tetragonal phase and the decomposition product CaHI was observed during cooling.

An overview of the compositions of the solid solutions and the temperature for X-ray data collection is presented in Table 4. The temperature region of existence for the observed solid solutions and their compositions is found in the supplementary information, Table s7.

**Table 4.** Compositions of the solid solutions found in the four investigated samples, **S1-S4**. The temperature for the X-ray data collections is given in parentheses. For sample S4 the iodide content is estimated from the volume of the compounds.

Compound	$x_{S1}$ (T / °C)	$x_{S2}$ (T / °C)	$x_{S3}$ (T / °C)	$x_{S4}$ (T / °C)
<i>tri</i> -Ca((BH <sub>4</sub> ) <sub>1-x</sub> I <sub>x</sub> ) <sub>2</sub>	0.39(44)	0.30(28)	-	~0.3(26)
<i>ort</i> -Ca((BH <sub>4</sub> ) <sub>1-x</sub> I <sub>x</sub> ) <sub>2</sub>	0.23(313)	0.36(322)	-	-
<i>tet</i> -Ca((BH <sub>4</sub> ) <sub>1-x</sub> I <sub>x</sub> ) <sub>2</sub>	0.65(361)	0.62(340)	0.61(170) <sup>a</sup>	~0.6(400)

<sup>a</sup> The compound forms during cooling of the sample.

It is noteworthy that the solid solution occurs with the distorted  $\beta$ -Ca(BH<sub>4</sub>)<sub>2</sub>, *ort*-Ca((BH<sub>4</sub>)<sub>1-x</sub>I<sub>x</sub>)<sub>2</sub>. Rietveld refinements reveal that the CaI<sub>2</sub> does not dissolve any  $\alpha$ -Ca(BH<sub>4</sub>)<sub>2</sub> upon heating of the ball milled mixtures (samples **S1** and **S2**). Therefore, the  $\alpha$ - to  $\alpha'$ -Ca(BH<sub>4</sub>)<sub>2</sub> phase transition is observed at similar temperatures as for pure  $\alpha$ -Ca(BH<sub>4</sub>)<sub>2</sub> (~222 °C) in all the heated Ca(BH<sub>4</sub>)<sub>2</sub>-CaI<sub>2</sub> mixtures.<sup>40</sup>

For the Ca(BH<sub>4</sub>)<sub>2</sub>-CaI<sub>2</sub> system iodide is the larger anion and CaI<sub>2</sub> was observed to dissolve significant amounts of the smaller anion BH<sub>4</sub><sup>-</sup>, *i.e.* Ca(BH<sub>4</sub>)<sub>2</sub>. This contrasts the behavior of LiBH<sub>4</sub>-LiCl system where BH<sub>4</sub><sup>-</sup> is the larger anion, and the hexagonal form of LiBH<sub>4</sub> readily dissolves the

alkali halide salts and stabilizes the hexagonal structure to ambient temperatures.<sup>35</sup> Notice, that there are no indications of any dissolution of  $\text{LiBH}_4$  in the alkali halide salts. Generally, the smaller anion tends to dissolve in the compound containing the larger anion, and the structure of the latter tends to be preserved in the obtained solid solution. This trend follows the relative size of the anions,  $\text{I}^- > \text{BH}_4^- > \text{Br}^- > \text{Cl}^-$  derived by a comparison of the unit cell volumes for different inorganic salts.<sup>61</sup> This trend in anion substitution reactions can be interpreted as an increase in the lattice energy due to the clearly observed decrease in the unit cell volume, *i.e.* a decrease in the average distance between the ions in the structure.

### 3.3 Thermal analysis of the new solid solutions.

Differential scanning calorimetry (DSC) and thermogravimetric analysis (TGA) measurements were conducted for  $\text{Ca}(\text{BH}_4)_2\text{-CaI}_2$  samples (**S1** and **S2**) and for  $\alpha\text{-Ca}(\text{BH}_4)_2$  (**R2**) and the data are shown in Figure 11 for the temperature range *RT* to 500 °C (heating rate of 10 °C/min). Calcium borohydride decomposes in several steps visible as endothermic peaks at 351, 379, and 437 °C in the DSC profile. All three peaks are associated with weight loss in accordance with previous reports.<sup>48,49,68</sup> The first hydrogen release is assigned to the decomposition of  $\beta\text{-Ca}(\text{BH}_4)_2$ , and the latter to the decomposition of intermediate phases with lower hydrogen contents.<sup>48</sup> The endothermic peaks are associated with a total mass loss of 5.46 wt% in the temperature range from 350 to 400 °C, which is less than the calculated gravimetric hydrogen content of  $\rho_m = 9.6$  wt%, possibly due to insufficient thermal treatment or air exposure.

Two almost coinciding peaks are observed in the DSC-profile for  $\text{Ca}(\text{BH}_4)_2\text{-CaI}_2$  (0.82 : 0.18, **S1**), at 384 and 388 °C, which supports the SR-PXD results, *i.e.* formation of  $\text{tet-Ca}((\text{BH}_4)_{0.35}\text{I}_{0.65})_2$  (361 °C, **S1**) followed by the decomposition to CaHI, which is observed in the temperature range 330 to

400 °C. The DSC-peaks are related to a total mass loss of 4.0 wt%, which is comparable to the expected gravimetric hydrogen content of  $\rho_m = 4.5$  wt% in the sample, see Table 5. On the other hand, a broad endothermic peak is observed at 385 °C associated with a mass loss of 2.75 wt% (calculated gravimetric hydrogen content  $\rho_m = 3.13$  wt%) for  $\text{Ca}(\text{BH}_4)_2\text{-CaI}_2$  (0.71 : 0.29, **S2**). This thermal event may be assigned to the formation of the tetragonal phase and the decomposition to  $\text{CaHI}$ . The decomposition temperature for samples **S1** and **S2** are detected at 388 and 385 °C, respectively, as compared to 379 °C for  $\alpha\text{-Ca}(\text{BH}_4)_2$  (**R2**). Therefore, the anion substitution may have a minor ‘stabilizing’ effect in the range 5 to 10 °C as compared to  $\alpha\text{-Ca}(\text{BH}_4)_2$ . The calculated volumetric and gravimetric hydrogen content of the substituted compounds is shown in the supplementary information Table s8.

### 3.4 Hydrogen release and uptake in the solid solutions $\text{Ca}(\text{BH}_4)_2\text{-CaI}_2$

Sieverts measurements were performed for  $\text{Ca}(\text{BH}_4)_2\text{-CaI}_2$  (0.71 : 0.29, **S2**) and for a reference sample of  $\alpha\text{-Ca}(\text{BH}_4)_2$  (**R2**). The desorption measurements were performed in vacuum in the temperature range  $RT$  to 550 °C (0.5 °C/min) and are shown in Figure 12. The desorption profile of  $\alpha\text{-Ca}(\text{BH}_4)_2$ , **R2**, contains at least four different hydrogen release rates starting at 200 °C with a maximum just above 300 °C. A total hydrogen release of 9.36 wt% is observed in accordance with the calculated gravimetric hydrogen content of  $\rho_m = 9.6$  wt%, see the reaction scheme (1). After rehydrogenation at 350 °C and  $p(\text{H}_2) = 100$  bar for 10 hours a second hydrogen desorption is measured for **R2** with a release of 2.16 wt%  $\text{H}_2$  observed in the temperature range  $RT$  to 550 °C, indicating that the sample was not fully loaded with hydrogen using the selected absorption conditions.

For  $\text{Ca}(\text{BH}_4)_2\text{-CaI}_2$  (0.71 : 0.29, **S2**) a relatively fast hydrogen release of 2.20 wt% is observed in the temperature range 320 to 360 °C followed by another distinct release step at 460 to 500 °C of 0.30 wt% giving a total hydrogen release of 3.50 wt%, which is larger than the calculated gravimetric hydrogen content of the sample of  $\rho_m = 3.13$  wt%. The observation of hydrogen release already at 320 °C indicates that the initial hydrogen desorption originates from the *ort*- $\text{Ca}((\text{BH}_4)_{1-x}\text{I}_x)_2$ .

The hydrogen desorption for the substituted sample, **S2**, occurs at 5 - 10 °C higher than for the pure  $\alpha\text{-Ca}(\text{BH}_4)_2$  consistent with the observations from the DSC/TGA. The results from DSC/TGA and from Sieverts measurements compared with the calculated  $\text{H}_2$  content are listed in Table 5.

**Table 5** The observed and the calculated mass loss ( $\rho_m$ ) from samples **S1**, **S2** and **R2** based on release of hydrogen.

Sample	DSC $T_{\text{dec}}/\text{°C}$	TGA obs. mass loss /wt%	PCT cycle 1 obs. mass loss /wt%	PCT cycle 2 obs. mass loss /wt%	$\rho_m(\text{H}_2)$ /wt%
<b>R2: Ca(BH<sub>4</sub>)<sub>2</sub></b>	379	5.46	9.30	2.16	9.60
<b>S1: Ca(BH<sub>4</sub>)<sub>2</sub>-CaI<sub>2</sub> (0.82 : 0.18)</b>	384	4.00	-	-	4.50
<b>S2: Ca(BH<sub>4</sub>)<sub>2</sub>-CaI<sub>2</sub> (0.71 : 0.29)</b>	385	2.75	3.50	0.81	3.13

#### 4. Conclusion

Anion substitution in the system  $\text{Ca}(\text{BH}_4)_2\text{-CaI}_2$  results in the formation of three new compounds, which are solid solutions with  $\text{BH}_4^-$  and  $\text{I}^-$  anions sharing the same positions in the structures. The sample preparation methods have a significant influence on the reaction pathway. Mechanochemical synthesis (ball milling) mediates a significant degree of dissolution of  $\text{Ca}(\text{BH}_4)_2$  in  $\text{CaI}_2$  yielding a  $\text{CaI}_2$ -type trigonal structure, *tri*- $\text{Ca}((\text{BH}_4)_{0.70}\text{I}_{0.30})_2$  (*RT*, **S2**). Thus, to a significant extend (~70%) iodide anions in  $\text{CaI}_2$  can be replaced by the  $\text{BH}_4^-$  anions mediated by ball milling. Upon

heating, *tri*-Ca((BH<sub>4</sub>)<sub>0.70</sub>I<sub>0.30</sub>)<sub>2</sub> (44 °C, **S2**) transforms to a CaCl<sub>2</sub>-type orthorhombic structure, *ort*-Ca((BH<sub>4</sub>)<sub>0.64</sub>I<sub>0.36</sub>)<sub>2</sub> (322 °C, **S2**), that is structurally related to the high-temperature form of calcium borohydride, β-Ca(BH<sub>4</sub>)<sub>2</sub>. Upon further heating (at 335 °C), the sample partly transforms to a more iodide-rich tetragonal solid solution is formed (~20 wt% of sample), *tet*-Ca((BH<sub>4</sub>)<sub>0.38</sub>I<sub>0.62</sub>)<sub>2</sub> (340 °C, **S2**), with a novel structure type. This compound decomposes to CaHI and CaB<sub>6</sub> (at  $T > 345$  °C). The heating of a hand-mixed Ca(BH<sub>4</sub>)<sub>2</sub>-CaI<sub>2</sub> sample reveals unidentified products and the *tet*-Ca((BH<sub>4</sub>)<sub>1-x</sub>I<sub>x</sub>)<sub>2</sub> at  $T > 300$  °C. In all cases, no indication of any uptake of CaI<sub>2</sub> in α-Ca(BH<sub>4</sub>)<sub>2</sub> was identified. Generally, the smaller anion tends to dissolve in the compound containing the larger anion, and the structure of the latter tends to be preserved in the obtained solid solution. A large structural diversity is observed within the Ca(BH<sub>4</sub>)<sub>2</sub>-CaI<sub>2</sub> system, which provides a unique decomposition pathway for the substituted compounds and possibly a minor stabilizing effect, *i.e.* 5 to 10 °C increase in hydrogen desorption temperatures.

## Acknowledgements

The European Commission (contract NMP-2008-261/FLYHY) and the Danish Research Council for Natural Sciences (Danskatt) is thanked for financial support. We are grateful to the competent team at the Swiss Norwegian Beam Line at ESRF for their assistance. The work was also supported by the Danish National Research Foundation (Centre for Materials Crystallography), the Danish Strategic Research Council (Centre for Energy Materials) and the Carlsberg Foundation.

## References

- (1) Ritter, J. A.; Ebner, A. D.; Wang, J.; Zidan, R. *Mater Today* **2003**, *6*, 18–23.
- (2) Schlapbach, L.; Züttel, A. *Nature* **2001**, *414*, 353–358.
- (3) Felderhoff, M.; Weidenthaler, C.; Helmolt, R.; Eberle, U. *Phys. Chem. Chem. Phys.* **2007**, *9*, 2643–2653.
- (4) U.S. Department of Energy DOE Targets for Onboard Hydrogen Storage Systems for Light-Duty Vehicles.  
[http://www1.eere.energy.gov/hydrogenandfuelcells/storage/pdfs/targets\\_onboard\\_hydro\\_storage.pdf](http://www1.eere.energy.gov/hydrogenandfuelcells/storage/pdfs/targets_onboard_hydro_storage.pdf).
- (5) Soloveichik, G. L. *Mater. Matt.* **2007**, *2*, 41944.
- (6) Orimo, S.; Nakamori, Y.; Eliseo, J. R.; Züttel, A.; Jensen, C. M. *Chem. Rev.* **2007**, *107*, 4111-4132.
- (7) Grochala, W.; Edwards, P. P. *Chem. Rev.* **2004**, *104*, 1283-1316.
- (8) Filinchuk, Y.; Chernyshov, D.; Dmitriev, V. Z. *Kristallogr.* **2008**, *223*, 649-659.
- (9) Hagemann, H.; Longhini, M.; Kaminski, J. W.; Wesolowski, T. A.; Černý, R.; Penin, N.; Sørby, M. H.; Hauback, B. C.; Severa, G.; Jensen, C. M. *J. Phys. Chem. A* **2008**, *112*, 7551-7555.
- (10) Černý, R.; Severa, G.; Ravnsbæk, D. B.; Filinchuk, Y.; D'Anna, V.; Hagemann, H.; Haase, D.; Jensen, C. M.; Jensen, T. R. *J. Phys. Chem. C* **2010**, *114*, 1357-1364.
- (11) Černý, R.; Ravnsbæk, D. B.; Severa, G.; Filinchuk, Y.; d'Anna, V.; Hagemann, H.; Haase, D.; Skibsted, J.; Jensen, C. M.; Jensen, T. R. *J. Phys. Chem. C* **2010**, *114*, 19540-19549.
- (12) Kim, C.; Hwang, S.; Bowman, R. C.; Reiter, J. W.; Zan, J. A.; Kulleck, J. G.; Kabbour, H.; Majzoub, E. H.; Ozolins, V. *J. Phys. Chem. C* **2009**, *113*, 9956-9968. (13) Ravnsbaek, D.; Filinchuk, Y.; Cerenius, Y.; Jakobsen, H. J.; Besenbacher, F.; Skibsted, J.; Jensen, T. R. *Angew. Chem. Int. Ed.* **2009**, *48*, 6659-6663.
- (14) Ravnsbæk, D. B.; Sørensen, L. H.; Filinchuk, Y.; Reed, D.; Book, D.; Jakobsen, H. J.; Besenbacher, F.; Skibsted, J.; Jensen, T. R. *Eur. J. Inorg. Chem.* **2010**, *11*, 1608-1612.
- (15) Jeon, E.; Cho, Y. W. *J. Alloys Compd.* **2006**, *422*, 273–275.
- (16) Kostka, J.; Lohstroh, W.; Fichtner, M.; Hahn, H. *J. Phys. Chem. C* **2007**, *111*, 14026-14029.
- (17) Hagemann, H.; D'Anna, V.; Carbonnière, P.; Gil Bardají, E.; Fichtner, M. *J. Phys. Chem. A* **2009**, *113*, 13932-13936.
- (18) Ravnsbæk, D. B.; Filinchuk, Y.; Černý, R.; Ley, M. B.; Haase, D.; Jakobsen, H. J.; Skibsted, J.; Jensen, T. R. *Inorg. Chem.* **2010**, *49*, 3801-3809.
- (19) Frommen, C.; Aliouane, N.; Deledda, S.; Fonnelløp, J. E.; Grove, H.; Lieutenant, K.; Llamas-Jansa, I.; Sartori, S.; Sørby, M. H.; Hauback, B. C. *J. Alloys Compd.* **2010**, *496*, 710-716.
- (20) Černý, R.; Penin, N.; Hagemann, H.; Filinchuk, Y. *J. Phys. Chem. C* **2009**, *113*, 9003-9007.
- (21) Černý, R.; Filinchuk, Y.; Hagemann, H.; Yvon, K. *Angew. Chem. Int. Ed.* **2007**, *46*, 5765-5767.
- (22) Lee, J. Y.; Ravnsbæk, D.; Lee, Y.; Kim, Y.; Cerenius, Y.; Shim, J.; Jensen, T. R.; Hur, N. H.; Cho, Y. W. *J. Phys. Chem. C* **2009**, *113*, 15080-15086.
- (23) Bösenberg, U.; Doppiu, S.; Mosegaard, L.; Barkhordarian, G.; Eigen, N.; Borgschulte, A.; Jensen, T. R.; Cerenius, Y.; Gutfleisch, O.; Klassen, T.; Dornheim, M.; Bormann, R. *Acta Mater.* **2007**, *55*, 3951–3958.
- (24) Bösenberg, U.; Kim, J. W.; Gossler, D.; Eigen, N.; Jensen, T. R.; von Colbe, J. M.; Zhou, Y.; Dahms, M.; Kim, D. H.; Günther, R.; Cho, Y. W.; Oh, K. H.; Klassen, T.; Bormann, R.; Dornheim, M. *Acta Mater.* **2010**, *58*, 3381-3389.
- (25) Vajo, J. J.; Skeith, S. L.; Mertens, F. *J. Phys. Chem. B* **2005**, *109*, 3719–3722.
- (26) Cho, Y. W.; Shim, J.; Lee, B. *Calphad* **2006**, *30*, 65–69.
- (27) Yin, L.; Wang, P.; Fang, Z.; Cheng, H. M. *Chem. Phys. Lett.* **2008**, *450*, 318-321.
- (28) Brinks, H. W.; Fossdal, A.; Hauback, B. C. *J. Phys. Chem. C* **2008**, *112*, 5658-5661.

- (29) Kang, X.; Wang, P.; Cheng, H. *Scripta Mater.* **2007**, *56*, 361-364.
- (30) Wang, P.; Kang, X.; Cheng, H. M. *ChemPhysChem* **2005**, *6*, 2488-2491.
- (31) Eigen, N.; Bösenberg, U.; Bellosta von Colbe, J.; Jensen, T. R.; Cerenius, Y.; Dornheim, M.; Klassen, T.; Bormann, R. *J. Alloys Compd.* **2009**, *477*, 76–80.
- (32) Hauback, B. C. *Z. Kristallogr.* **2008**, *223*, 636–648.
- (33) Maekawa, H.; Matsuo, M.; Takamura, H.; Ando, M.; Noda, Y.; Karahashi, T.; Orimo, S. *J. Am. Chem. Soc.* **2009**, *131*, 894-895.
- (34) Mosegaard, L.; Møller, B.; Jorgensen, J.; Filinchuk, Y.; Cerenius, Y.; Hanson, J. C.; Dimasi, E.; Besenbacher, F.; Jensen, T. R. *J. Phys. Chem. C* **2008**, *112*, 1299-1303.
- (35) Arnbjerg, L. M.; Ravnsbæk, D. B.; Filinchuk, Y.; Vang, R. T.; Cerenius, Y.; Besenbacher, F.; Jørgensen, J.; Jakobsen, H. J.; Jensen, T. R. *Chem. Mater.* **2009**, *21*, 5772-5782.
- (36) Lee, J. Y.; Lee, Y.; Suh, J.; Shim, J.; Cho, Y. W. *J. Alloys Compd.* **2010**, *506*, 721-727.
- (37) Rönnebro, E.; Majzoub, E. H. *J. Phys. Chem. B* **2007**, *111*, 12045-12047.
- (38) Miwa, K.; Aoki, M.; Noritake, T.; Ohba, N.; Nakamori, Y.; Towata, S.; Züttel, A.; Orimo, S. *Phys. Rev. B* **2006**, *74*, 155122.
- (39) Kim, J.; Jin, S.; Shim, J.; Cho, Y. W. *Scripta Mater.* **2008**, *58*, 481-483.
- (40) Filinchuk, Y.; Rönnebro, E.; Chandra, D. *Acta Mater* **2009**, *57*, 732–738.
- (41) Buchter, F.; Łodziana, Z.; Remhof, A.; Friedrichs, O.; Borgschulte, A.; Mauron, P.; Züttel, A.; Sheptyakov, D.; Barkhordarian, G.; Bormann, R.; Chłopek, K.; Fichtner, M.; Sørby, M.; Riktor, M.; Hauback, B.; Orimo, S. *J. Phys. Chem. B* **2008**, *112*, 8042-8048.
- (42) Aoki, M.; Miwa, K.; Noritake, T.; Ohba, N.; Matsumoto, M.; Li, H.; Nakamori, Y.; Towata, S.; Orimo, S. *Appl. Phys. A* **2008**, *92*, 601-605.
- (43) Barkhordarian, G.; Jensen, T. R.; Doppiu, S.; Bösenberg, U.; Borgschulte, A.; Gremaud, R.; Cerenius, Y.; Dornheim, M.; Klassen, T.; Bormann, R. *J. Phys. Chem. C* **2008**, *112*, 2743-2749.
- (44) Lee, Y.; Kim, Y.; Cho, Y.; Shapiro, D.; Wolverton, C.; Ozoliņš, V. *Phys. Rev. B* **2009**, *79*.
- (45) Buchter, F.; Łodziana, Z.; Remhof, A.; Friedrichs, O.; Borgschulte, A.; Mauron, P.; Züttel, A.; Sheptyakov, D.; Palatinus, L.; Chłopek, K.; Fichtner, M.; Barkhordarian, G.; Bormann, R.; Hauback, B. C. *J. Phys. Chem. C* **2009**, *113*, 17223-17230.
- (46) Noritake, T.; Aoki, M.; Matsumoto, M.; Miwa, K.; Towata, S.; Li, H.; Orimo, S. *J. Alloys Compd.* **2010**, *491*, 57-62.
- (47) Fichtner, M.; Chłopek, K.; Longhini, M.; Hagemann, H. *J. Phys. Chem. C* **2008**, *112*, 11575-11579.
- (48) Riktor, M. D.; Sørby, M. H.; Chłopek, K.; Fichtner, M.; Buchter, F.; Züttel, A.; Hauback, B. C. *J. Mater. Chem.* **2007**, *17*, 4939-4942.
- (49) Kim, Y.; Reed, D.; Lee, Y.; Lee, J. Y.; Shim, J.; Book, D.; Cho, Y. W. *J. Phys. Chem. C* **2009**, *113*, 5865-5871.
- (50) Kim, J.; Shim, J.; Cho, Y. W. *J Power Sources* **2008**, *181*, 140-143.
- (51) Jensen, T. R.; Nielsen, T. K.; Filinchuk, Y.; Jørgensen, J. E.; Cerenius, Y.; Gray, E. M.; Webb, C. J. *J. Appl. Cryst.* **2010**, *43*, 1456-1463.
- (52) Hammersley, A. P.; Svensson, S. O.; Hanfland, M.; Fitch, A. N.; Hausermann, D. *High Pressure Res* **1996**, *14*, 235–248.
- (53) Vogel, S.; Ehm, L.; Knorr, K.; Braun, C. *Adv. X-ray Anal.* **2002**, *45*, 31-33.
- (54) Boulton, A.; Louër, D. *J. Appl. Cryst.* **2004**, *37*, 724-731.
- (55) Favre-Nicolin, V.; Cerný, R. *J. Appl. Cryst.* **2002**, *35*, 734-743.
- (56) Rodriguez-Carvajal, J. *FULLPROF SUITE: LLB Sacley & LCSIM Rennes; France*, **2003**.
- (57) Blum, H. Z. *Phys. Chem. B-Chem. E* **1933**, *22*, 298-304.
- (58) Ehrlich, P.; Kulke, H. Z. *Anorg. Allg. Chem.* **1956**, *288*, 156-170.
- (59) Busing, W. R. *T. Am. Cryst.* **1970**, *6*, 57-72.
- (60) PCTPro-2000 - Calorimetry and thermal analysis, <http://www.setaram.com/PCTPro-2000.htm>.

- (61) Filinchuk, Y.; Hagemann, H. *Eur. J. Inorg. Chem.* **2008**, *20*, 3127-3133.
- (62) Howard, C. J.; Kennedy, B. J.; Curfs, C. *Phys. Rev. B* **2005**, *72*, 214114.
- (63) Brostigen, G.; Kjekshus, A. *Acta Chem. Scand.* **1970**, *24*, 1925-1940.
- (64) Abrahams, S. C.; Schmalle, H. W.; Williams, T.; Reller, A.; Lichtenberg, F.; Widmer, D.; Bednorz, J. G.; Spreiter, R.; Bosshard, C.; Günter, P. *Acta Crystallogr. B Struct. Sci.* **1998**, *54*, 399-416.
- (65) Filinchuk, Y.; Chernyshov, D.; Nevidomskyy, A.; Dmitriev, V. *Angew. Chem. Int. Ed.* **2008**, *47*, 529-532.
- (66) Majzoub, E. H.; Rönnebro, E. *J. Phys. Chem. C* **2009**, *113*, 3352-3358.
- (67) Balema, V. P. *Mater. Matt.* **2007**, *2*, 16-18.
- (68) Kim, J.; Jin, S.; Shim, J.; Cho, Y. W. *J. Alloys Compd.* **2008**, *461*, L20-L22.

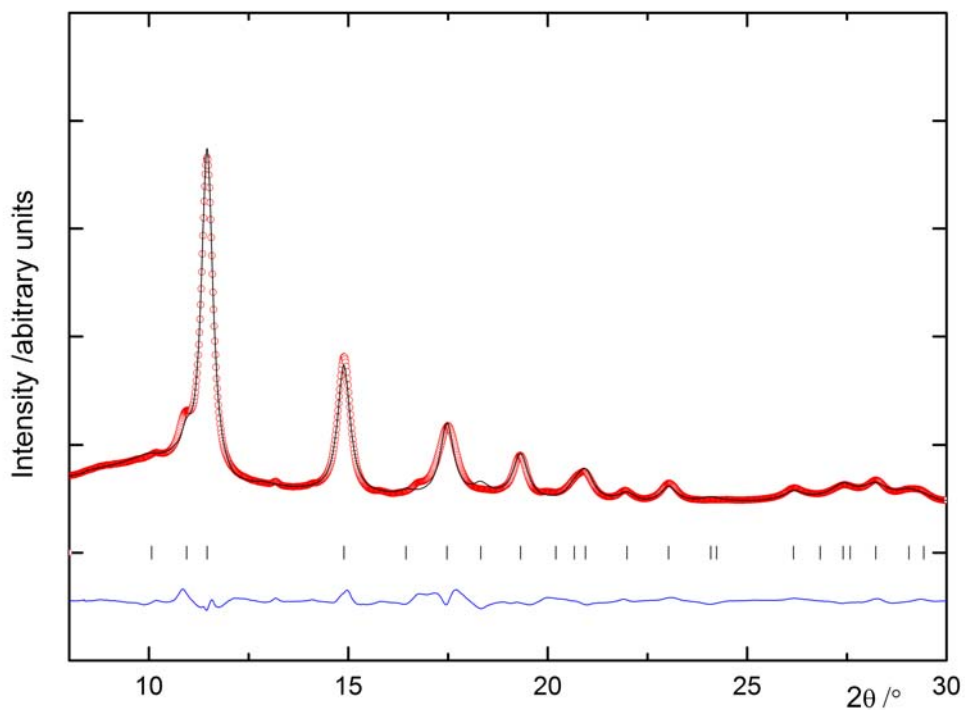


**Figure 1** Rietveld refinement profile of a new  $\text{CaI}_2$ -type trigonal compound,  $\text{tri-Ca}((\text{BH}_4)_{0.70}\text{I}_{0.30})_2$ , space group  $P\bar{3}m1$ , formed by ball milling sample **S2**. The red circles depict the observed data and the black line shows the calculated fit. The difference plot is shown in blue. The data was collected at 28 °C, using  $\lambda = 0.6548 \text{ \AA}$ .

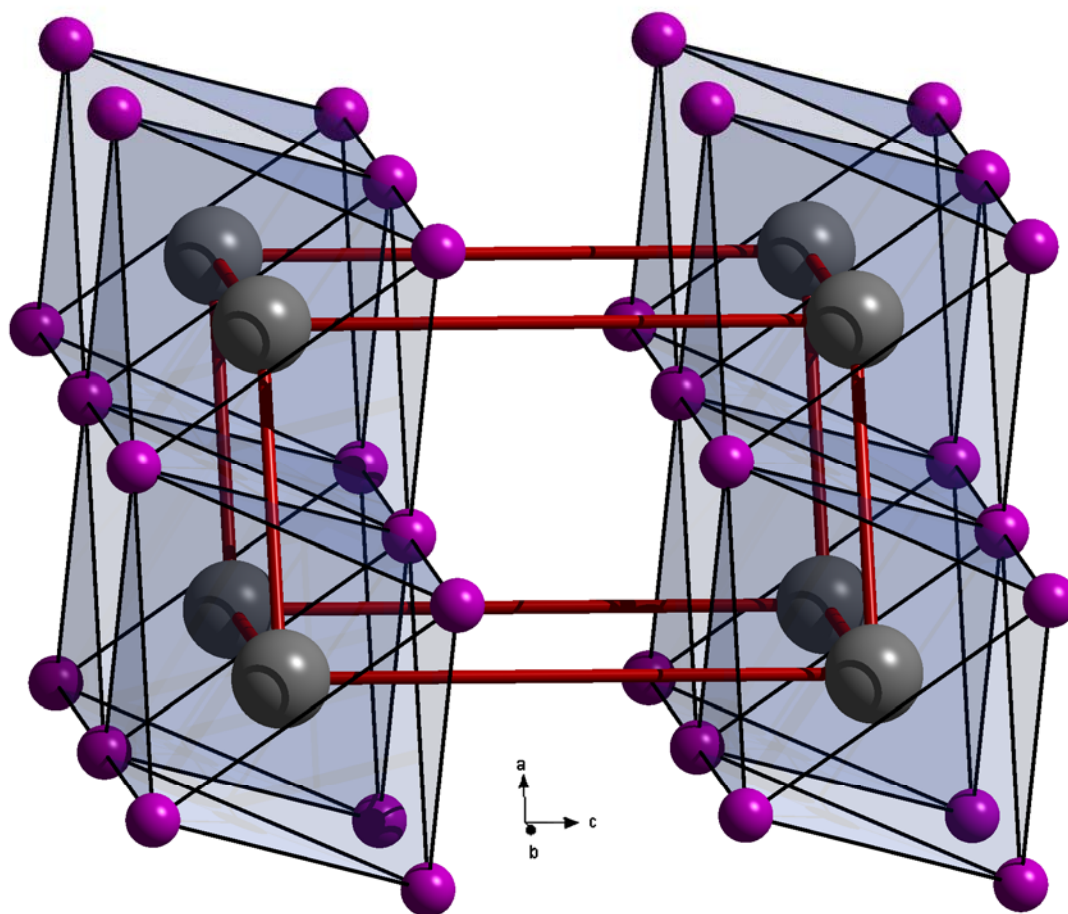


**Figure 2** Crystal structure of a new CaI<sub>2</sub>-type trigonal compound, *tri*-Ca((BH<sub>4</sub>)<sub>0.70</sub>I<sub>0.30</sub>)<sub>2</sub>. The calcium atoms are shown in grey and I<sup>-</sup> and BH<sub>4</sub><sup>-</sup>, obtaining the same positions, are shown as purple spheres.

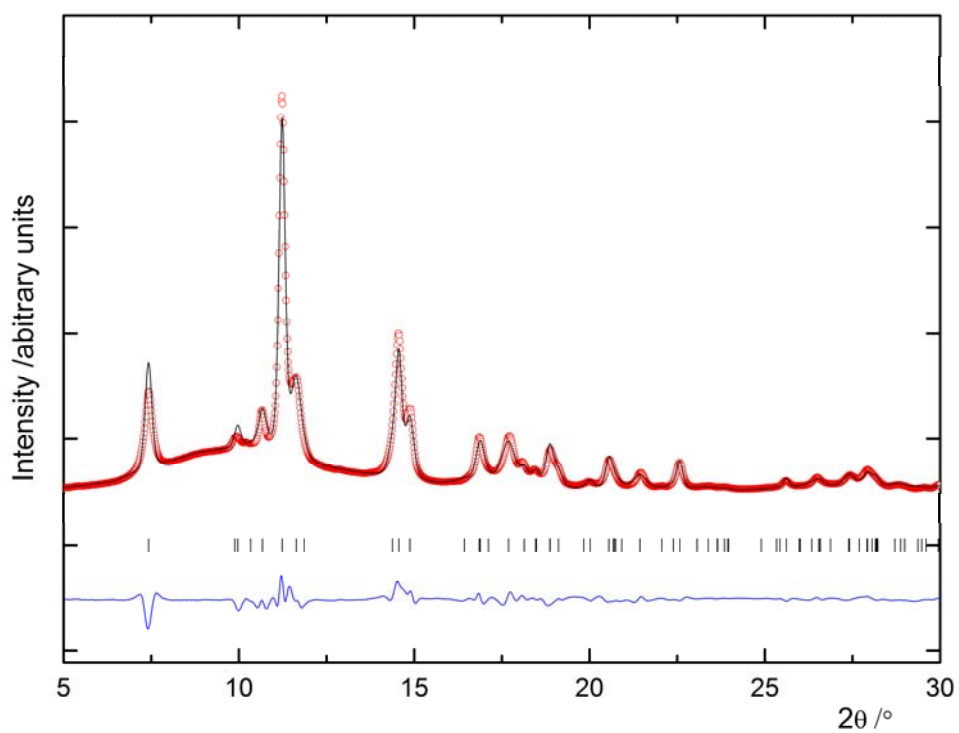


**Figure 3** Rietveld refinement profile of a new  $\text{CaCl}_2$ -type orthorhombic structure, *ort*- $\text{Ca}((\text{BH}_4)_{0.64}\text{I}_{0.36})_2$ , space group  $Pnmm$ , formed by heating sample **S2** to 322 °C. The red circles depict the observed data and the black line shows the calculated fit. The difference plot is shown in blue. The data was collected at 322 °C, using  $\lambda = 0.6548 \text{ \AA}$ .

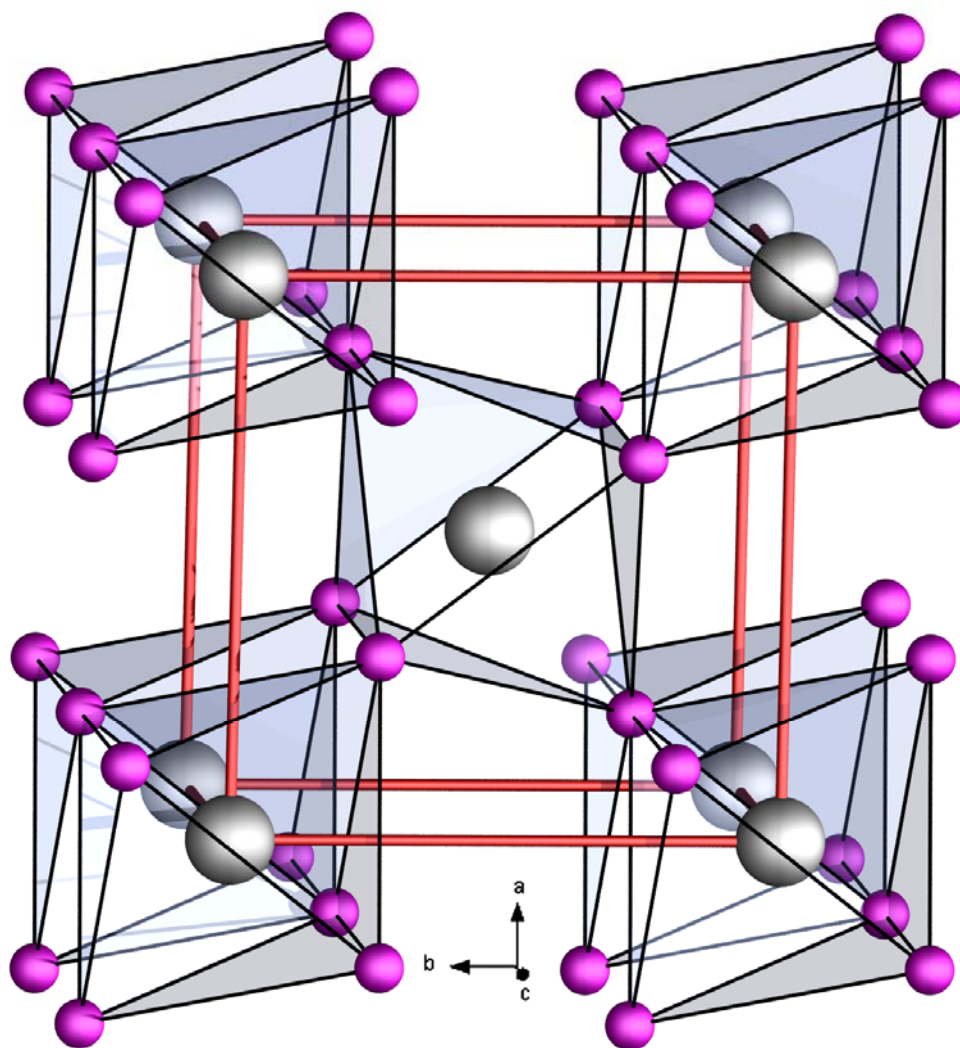


**Figure 4** Crystal structure of a new CaCl<sub>2</sub>-type orthorhombic structure, *ort*-Ca((BH<sub>4</sub>)<sub>0.64</sub>I<sub>0.36</sub>)<sub>2</sub>. The calcium atoms are shown in grey and I<sup>-</sup> and BH<sub>4</sub><sup>-</sup>, occupying the same position, are marked as purple spheres.

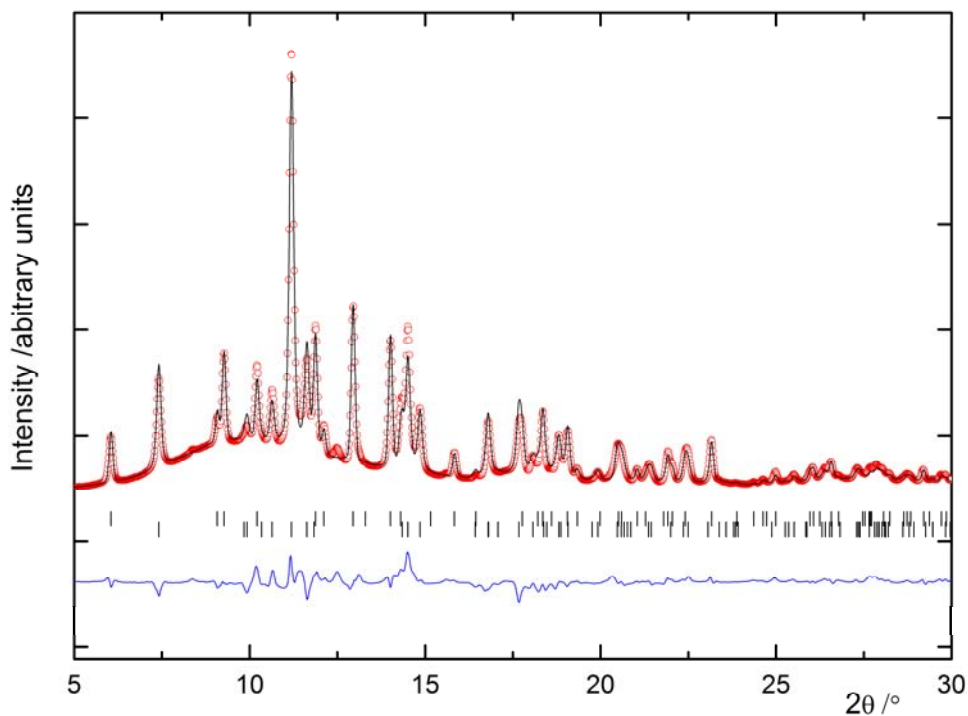


**Figure 5** Rietveld refinement profile of a new tetragonal structure,  $tet\text{-Ca}((\text{BH}_4)_{0.38}\text{I}_{0.62})_2$ , space group  $I4mm$ , formed by heating sample **S2** to 340 °C. The sample contains only 20 wt% of this phase and 80 wt% of the orthorhombic  $ort\text{-Ca}((\text{BH}_4)_{0.61}\text{I}_{0.39})_2$   $\text{CaCl}_2$ -type structure (lower tick marks). The red circles depict the observed data and black line shows the calculated fit. The difference plot is shown in blue. The data was collected at 340 °C using  $\lambda = 0.6548 \text{ \AA}$ .

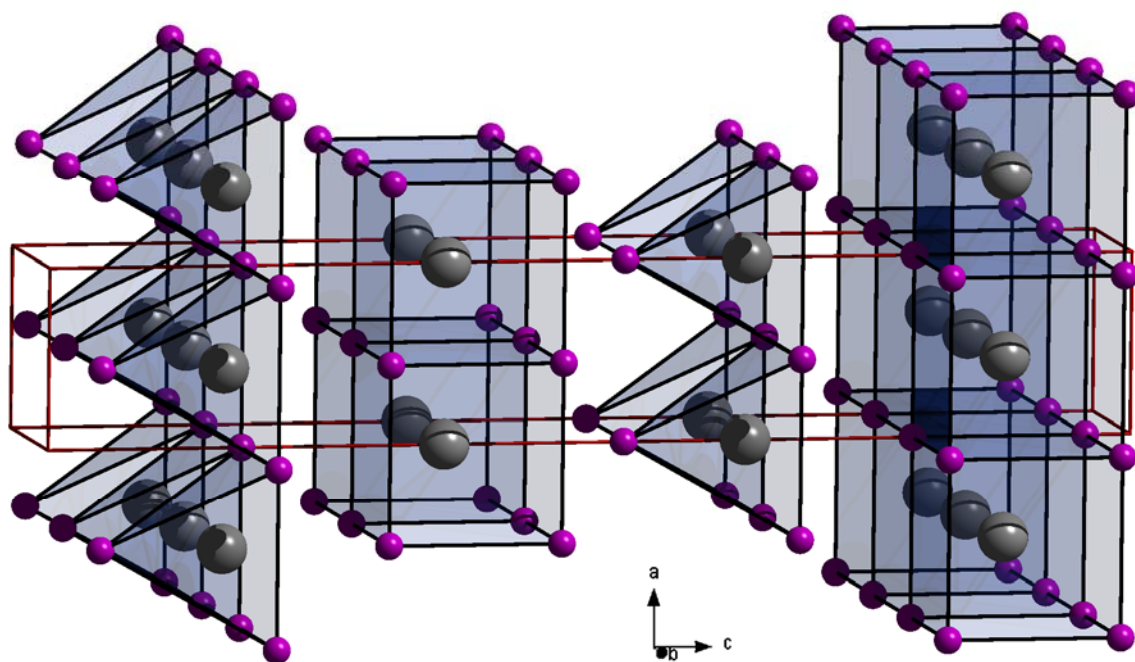


**Figure 6** Crystal structure of tetragonal,  $tet\text{-Ca}((\text{BH}_4)_{0.38}\text{I}_{0.62})_2$ . The calcium atoms are shown as grey spheres and the anions are shown as purple spheres. The space group is  $I4mm$ , and the cell parameters are  $a = 4.110$  and  $c = 24.845 \text{ \AA}$  at  $T = 340 \text{ }^\circ\text{C}$ .

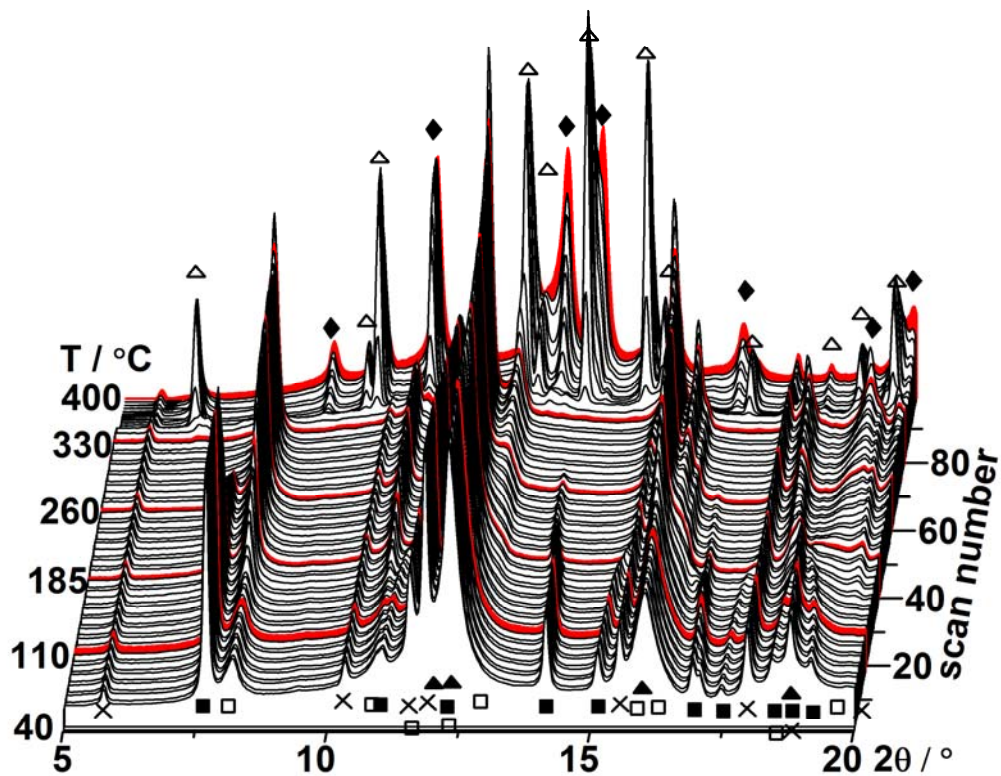


**Figure 7** *In situ* SR-PXD data measured for  $\text{Ca}(\text{BH}_4)_2\text{-CaI}_2$  (0.82 : 0.18, S1) heated from *RT* to 400 °C (heating rate 2 °C/min,  $\lambda = 0.703511 \text{ \AA}$ ). Symbols: ■  $\alpha\text{-Ca}(\text{BH}_4)_2$  and  $\alpha'\text{-Ca}(\text{BH}_4)_2$ , ×  $\text{CaI}_2$ , ▲ *tri*- $\text{Ca}((\text{BH}_4)_{1-x}\text{I}_x)_2$ , □ *ort*- $\text{Ca}((\text{BH}_4)_{1-x}\text{I}_x)_2$ , △ *tet*- $\text{Ca}((\text{BH}_4)_{1-x}\text{I}_x)_2$ , and ◆  $\text{CaHI}$ .

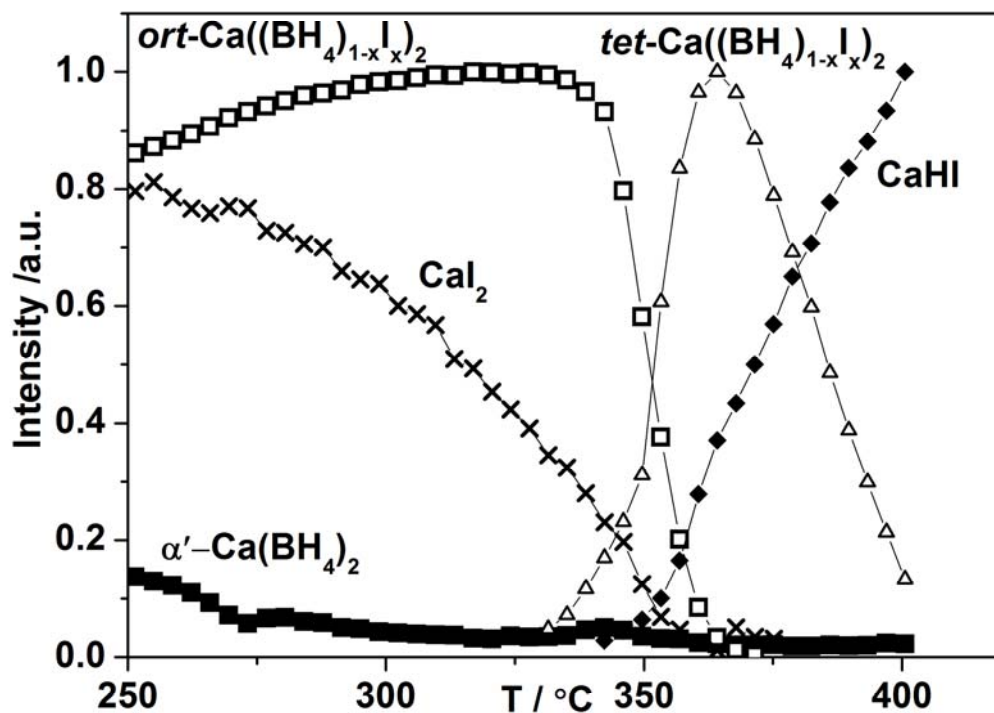


**Figure 8** Normalized and integrated intensities for the temperature range 250 to 400 °C of the *in situ* SR-PXD data measured for Ca(BH<sub>4</sub>)<sub>2</sub>-CaI<sub>2</sub> (0.82 : 0.18, S1), see Figure 7. Symbols: ■  $\alpha'$ -Ca(BH<sub>4</sub>)<sub>2</sub>, × CaI<sub>2</sub>, □ *ort*-Ca((BH<sub>4</sub>)<sub>1-x</sub>I<sub>x</sub>)<sub>2</sub>, △ *tet*-Ca((BH<sub>4</sub>)<sub>1-x</sub>I<sub>x</sub>)<sub>2</sub>, and ◆ CaHI. Please notice that the beginning of the experiment is not shown.

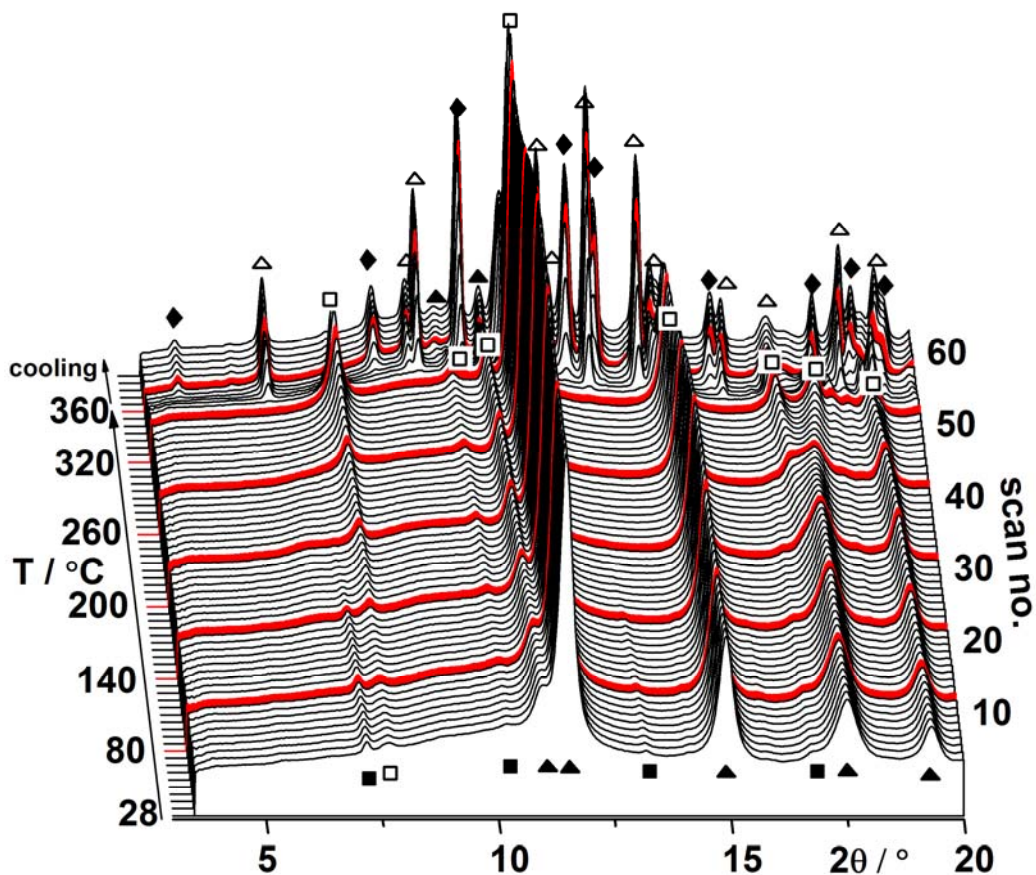


**Figure 9** *In situ* SR-PXD data measured for  $\text{Ca}(\text{BH}_4)_2\text{-CaI}_2$  (0.71 : 0.29, S2) heated from *RT* to 360 °C (heating rate 3 °C/min,  $\lambda = 0.6548 \text{ \AA}$ ). Symbols:  $\blacksquare$   $\alpha\text{-Ca}(\text{BH}_4)_2$ ,  $\blacktriangle$  *tri*- $\text{Ca}((\text{BH}_4)_{1-x}\text{I}_x)_2$ ,  $\square$  *ort*- $\text{Ca}((\text{BH}_4)_{1-x}\text{I}_x)_2$ ,  $\triangle$  *tet*- $\text{Ca}((\text{BH}_4)_{1-x}\text{I}_x)_2$ , and  $\blacklozenge$   $\text{CaHI}$ .

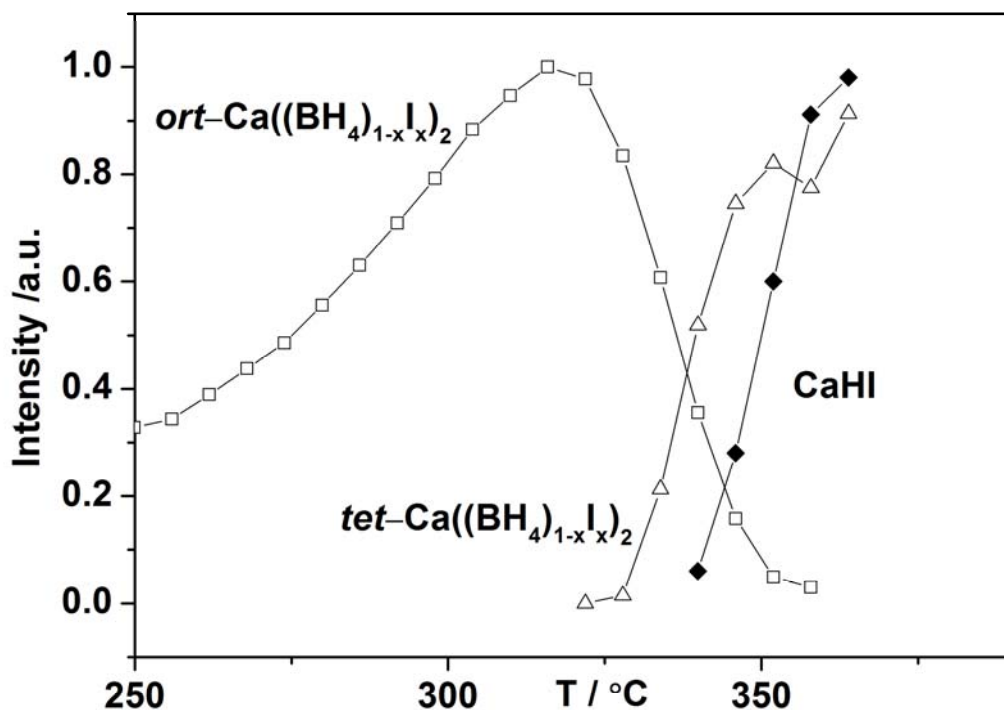


**Figure 10** Normalized and integrated intensities for the temperature range 250 to 360 °C of the *in situ* SR-PXD data measured for Ca(BH<sub>4</sub>)<sub>2</sub>-CaI<sub>2</sub> (0.71 : 0.29, S2), see Figure 9. Symbols: □ *ort*-Ca((BH<sub>4</sub>)<sub>1-x</sub>I<sub>x</sub>)<sub>2</sub>, △ *tet*-Ca((BH<sub>4</sub>)<sub>1-x</sub>I<sub>x</sub>)<sub>2</sub>, and ◆ CaHI.

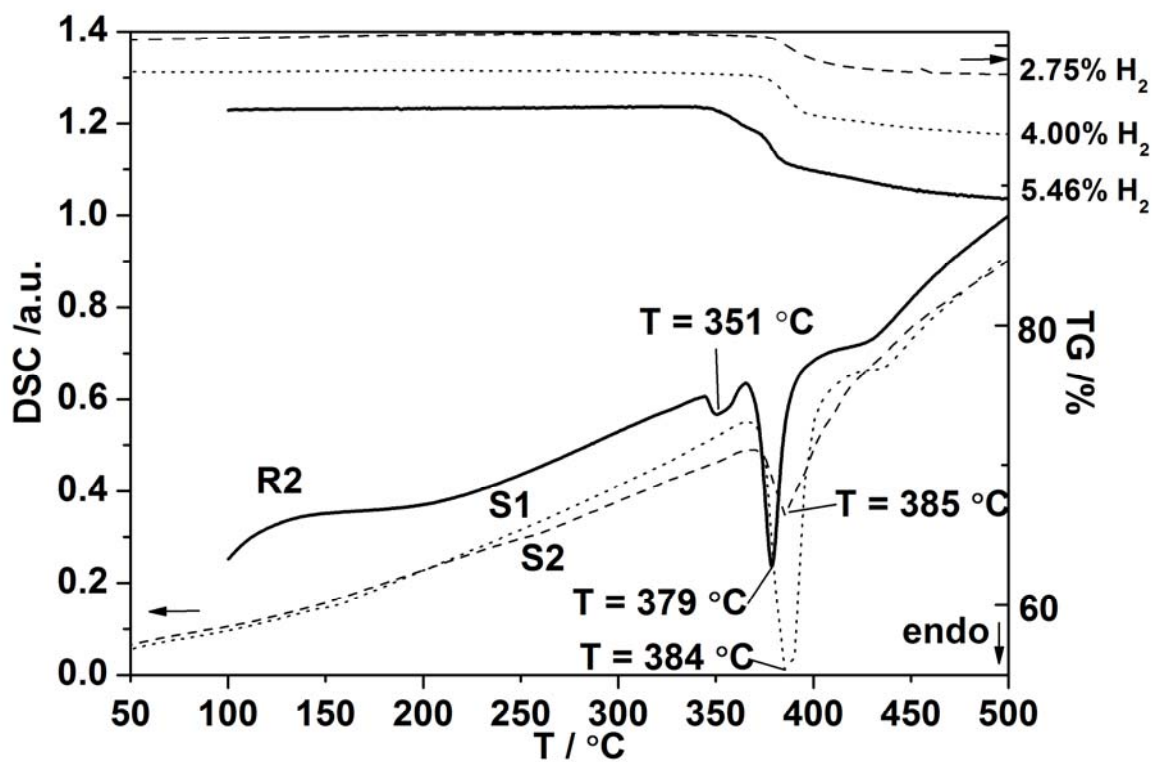


**Figure 11** Thermal analysis (DSC and TGA) for  $\text{Ca}(\text{BH}_4)_2\text{-CaI}_2$  (0.82 : 0.18, **S1**, dotted line),  $\text{Ca}(\text{BH}_4)_2\text{-CaI}_2$  (0.71 : 0.29, **S2**, dashed line) and  $\alpha\text{-Ca}(\text{BH}_4)_2$  (**R2**, solid line). The DSC data are normalized for comparison (heating rate 10 °C/min).

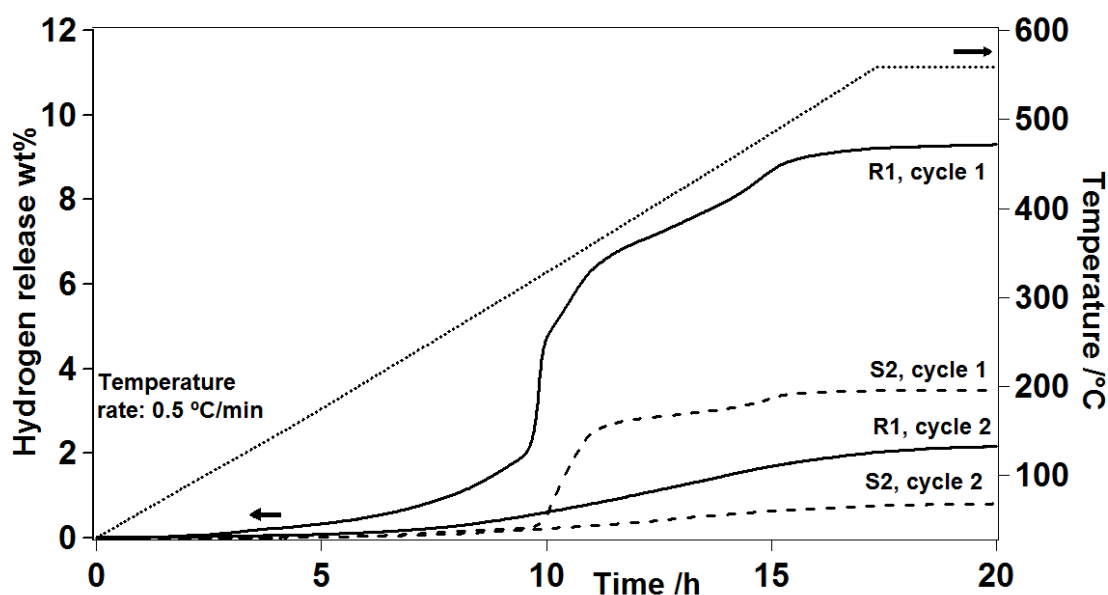


**Figure 12** Two cycles of TPD measurements for  $\text{Ca}(\text{BH}_4)_2\text{-CaI}_2$  (0.71 : 0.29, **S2**, dashed line) and  $\alpha\text{-Ca}(\text{BH}_4)_2$  (**R2**, solid line) heated from *RT* to 550 °C (heating rate 0.5 °C/min) is displayed as hydrogen release (wt%) versus time (h). The temperature profile is displayed as dots, and the temperature scale is shown in the right side of the figure.